JACS
JOURNAL OF THE AMERICAN CHEMICAL SOCIETY
pubs.acs.org/JACS
Article

Modular Design of G-Quadruplex MetalloDNAzymes for Catalytic C–C Bond Formations with Switchable Enantioselectivity

Philip M. Punt, Marie D. Langenberg, Okan Altan, and Guido H. Clever*

Cite This: J. Am. Chem. Soc. 2021, 143, 3555–3561
Read Online
ACCESS | Metrics & More | Article Recommendations | Supporting Information

ABSTRACT: Metal-binding DNA structures with catalytic function are receiving increasing interest. Although a number of metalloDNAzymes have been reported to be highly efficient, the exact coordination/position of their catalytic metal center is often unknown. Here, we present a new approach to rationally develop metalloDNAzymes for Lewis acid-catalyzed reactions such as enantioselective Michael additions. Our strategy relies on the predictable folding patterns of unimolecular DNA G-quadruplexes, combined with the concept of metal-mediated base-pairing. Transition-metal coordination environments were created in G-quadruplex loop regions, accessible by substrates. Therefore, protein-inspired imidazole ligandoside **L** was covalently incorporated into a series of G-rich DNA strands by solid-phase synthesis. Iterative rounds of DNA sequence design and catalytic assays allowed us to select tailored metalloDNAzymes giving high conversions and excellent enantioselectivities (≥99%). Based on their primary sequence, folding pattern, and metal coordination mode, valuable information on structure–activity relationships could be extracted. Variation of the number and position of ligand **L** within the sequence allowed us to control the formation of (*S*) and (*R*) enantiomeric reaction products, respectively.

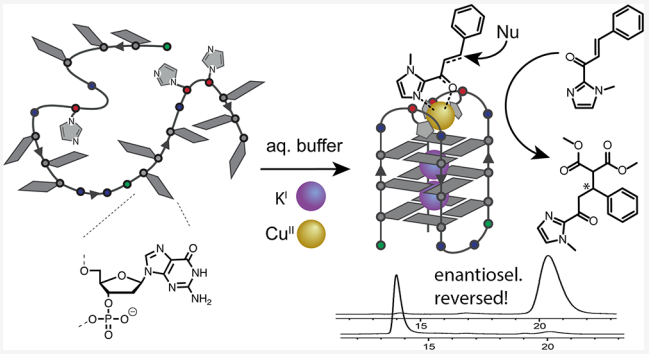

INTRODUCTION

Proteins have evolved over billions of years for countless processes, including regulatory, structural, and catalytic functions. Roughly half of the proteins need transition-metal cations for their correct folding and function. Which purpose this metal serves largely relies on its redox properties, spin state, and Lewis acidity, fine-tuned by highly conserved coordination environments.[1]

Owing to their high efficiencies and selectivities, metalloenzymes form the basis of numerous biotechnological applications.[2] The development of strategies to improve and redesign metalloenzymes consisting of a protein scaffold and a metal cofactor is a vibrant research field. For anchoring metal cofactors inside an engineered protein, different covalent and non-covalent strategies have been established: (a) coordination of an unsaturated metal complex,[3] (b) metal substitution,[4] (c) supramolecular anchoring, e.g., with a high-affinity tag,[5] and (d) covalent immobilization.[6] In this way, a vast number of artificial enzymes has been created to catalyze reactions such as oxime formation, carbene transfer, cyclopropanation, imine reduction, and ring-closing metathesis.[5−9]

In the past decades, a growing interest developed to expand the concept of engineered or artificial metalloenzymes to catalytically active oligonucleotides. In the context of single-stranded DNA sequences that catalyze the cleavage or ligation of other nucleic acids, the term "DNAzyme" (portmanteau of "DNA" and "enzyme") was coined in the 1990s.[10,11] Over the years, the scope of accepted substrates and reaction types could be greatly enhanced.[12−15]

With respect to transition-metal-containing oligonucleotides with rate-enhancing function, a major challenge remains anchoring the catalytic center in a precise and predetermined position. While proteins feature several amino acids to coordinate or tether a metal complex, the four canonical nucleobases of DNA offer only limited possibilities. As a solution, chelate ligands were bound to DNA via covalent or non-covalent interactions. In this way, peroxidase-like reactions and Zn^{II}- and Ce^{IV}-dependent site-specific RNA and DNA cleavage were established.[16−18] Roelfes and Feringa pioneered the design of Cu^{II} complexes that bind to double-stranded DNA for enantioselective transformations such as Diels–Alder reactions, Michael additions, and Friedel–Crafts reactions.[19−23] In recent times, also DNA G-quadruplexes were discovered for chiral catalysis, and a first example was reported in 2010 by Moses et al. They showcased an enantioselective Diels–Alder reaction by planar Cu^{II} chelates, non-covalently

Received: December 22, 2020
Published: February 25, 2021

https://dx.doi.org/10.1021/jacs.0c13251
J. Am. Chem. Soc. 2021, 143, 3555–3561

stacked on a terminal G-quartet.[24] Later, Wang and Li demonstrated Friedel–Crafts reactions, cyclopropanations, and other transformations. Most interestingly, they observed a case of switchable enantioselectivity, depending on the electrolyte composition, containing either Na^+ or K^+.[25−29] Whereas previous approaches were based on non-covalently bound metal complexes, Jäschke et al. introduced covalently connected bipyridine ligands into G-quadruplexes to catalyze Michael additions in good to excellent enantiomeric excesses (*ee*). Interestingly, enantioselectivity could be reversed by changing the position.[30]

Although high efficiencies and selectivities were obtained in these studies, the exact localization/orientation of the metal center with respect to the oligonucleotide secondary structure remained either out of direct control or even largely unknown, making deeper systematic studies a challenging task. In contrast, the field of "metal-mediated base-pairing", describing the incorporation of metal cations in precisely defined DNA coordination environments by replacing hydrogen-bonded base interactions, opened a new level of structural control over such bio-artificial hybrids owing to its systematic development in the past 20 years. Certain combinations of canonical nucleobases as well as DNA-incorporated artificial surrogates were shown to allow selective binding of metal cations such as Hg^{II}, Cu^{II}, Mn^{II}, Ag^{I}, Zn^{II}, and more,[31−34] culminating in programmable mixed-metal wires with potential application in nanotechnology.[35]

Recently, the concept was expanded from duplex DNA to higher structures, such as three-way junctions,[36] triplex DNA,[37] and i-motifs.[38] Our lab has focused on G-quadruplexes,[39,40] assembling from guanine-rich sequences via Hoogsteen base-pairing within π-stacked G-tetrads, stabilized by central cations, usually Na^+ or K^+.[41,42] We reported the first example of a metal-mediated tetramolecular G-quadruplex in 2013.[39] This was later expanded to unimolecular G-quadruplexes, and the concept was applied for the design of Cu^{II}-based EPR-distance rulers and Cu^{II}-responsive DNAzymes with peroxidase activity.[43−46]

Previously, we used unimolecular G-quadruplexes as templates for the incorporation of glycol-based imidazole ligandoside **L** to design tailored coordination environments for different transition-metal cations (Figure 1).[47,48] **L** was covalently incorporated as a glycerol nucleic acid (GNA) building block in both enantiomeric forms (*R*/*S*, $\mathbf{L}^{R/S}$) in the DNA backbone by replacement of a G-tetrad or loop bases (Figure 1). Here we show how the concept can be used for the rational design and optimization of metalloDNAzymes catalyzing a Cu^{II}-dependent Michael addition with tunable enantioselectivity.[49]

RESULTS AND DISCUSSION

Sequence Design and Initial Screen. Our design followed two considerations. First, a coordinatively unsaturated Cu^{II} center was deemed necessary to enable substrate activation, limiting the number of **L** to ≤3. Second, proximity of all incorporated ligands was crucial to enable Cu^{II} chelation. Based on the sequence of the human telomeric repeat $htel_{22}$ (AGG GTT AGG GTT AGG GTT AGG G; **L** replaces underlined nucleotides), we designed sequences htel$\mathbf{L}^S_2$A and htel$\mathbf{L}^S_3$A with the *S*-enantiomer of **L** ($\mathbf{L}^S$) incorporated into loops 1 and 3 (Figure 1, Supporting Information (SI) Table S2). To test our concept, we performed Michael additions of acceptor **MA1** with dimethyl malonate (DMM, see Table 1 for details).[36] Indeed, Cu^{II} complexes of htel$\mathbf{L}^S_2$A and htel$\mathbf{L}^S_3$A were found to catalyze the reaction as compared to unmodified $htel_{22}$, however, showing low conversions and enantioselectivities. Pleasingly, opposite product enantiomers were formed (htel$\mathbf{L}^S_2$A: 31% *ee* (*S*); htel$\mathbf{L}^S_3$A: 31% *ee* (*R*)), illustrating the potential to design tailored metalloDNAzymes for accessing both enantiomers without having to reverse stereochemistry in the DNA backbone. To test whether coordinatively unsaturated Cu^{II} was mandatory, we screened a series of sequences containing ≥4 counts of $\mathbf{L}^S$, indeed all showing poor conversion and *ee* values.

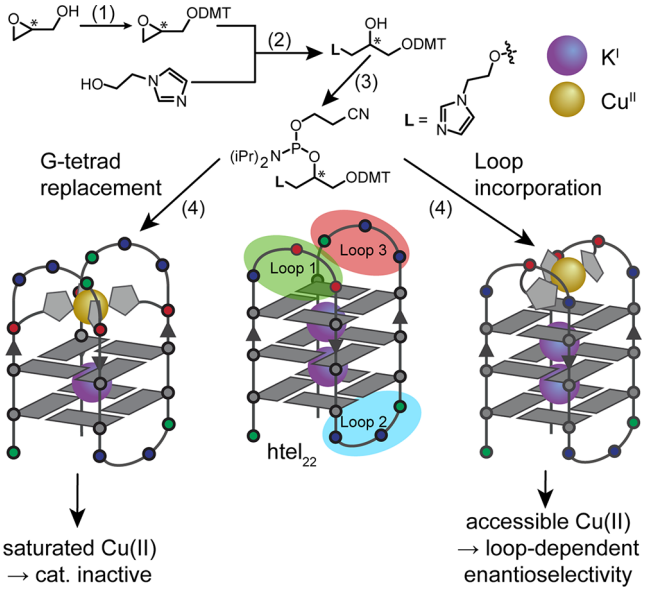

Figure 1. (a) Synthesis of imidazole ligandoside **L**. Conditions: (1) DMT-Cl, Et_3N in CH_2Cl_2; (2) NaH in DMF, 40 °C; (3) CEDIP-Cl, DIPEA in CH_2Cl_2, rt; (4) solid-phase DNA synthesis. Green, adenosine; blue, thymidine; gray, guanosine; and red, **L**.

Table 1. Screening of Different G-Quadruplex-Forming Sequences with 0–6 Counts of L[a]

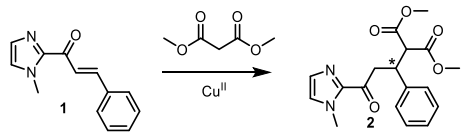

sequence	L	conversion (%)	*ee* (%)
Cu^{II} only	–	23 (±1)	0
N-Me-imidazole (4 equiv)	–	30 (±1)	0
$\mathbf{L}^S$ (4 equiv)	4	24 (±3)	1 (*S*) (±3)
$htel_{22}$	0	10 (±1)	5 (*S*) (±7)
htel$\mathbf{L}^S_2$A	2	28 (±2)	31 (*S*) (±1)
htel$\mathbf{L}^S_3$A	3	28 (±6)	31 (*R*) (±1)
htel$\mathbf{L}^S_4$A	4	10 (±1)	25 (*R*) (±2)
htel$\mathbf{L}^S_6$	6	0	0

[a]Conditions: 120 μM G-quadruplex, 100 μM $CuSO_4$, 10 mM HEPES pH 8, 100 mM KCl, 100 mM DMM, 1 mM **MA1**, and 1% v/v DMSO, 5 °C, 3 d. All experiments were performed in duplicate. The reported error is the standard deviation from two experiments.

Altered Sequences for Optimized Catalytic Performance. Encouraged by these results, a series of sequences with two or three $\mathbf{L}^S$ in loops 1 and 3 was synthesized, keeping a constant loop length of three bases. Catalytic studies unveiled crucial structure–function relationships for certain groups of

https://dx.doi.org/10.1021/jacs.0c13251
J. Am. Chem. Soc. 2021, 143, 3555−3561

sequences. One group containing three $\mathbf{L}^S$, one in loop 1 and two in loop 3, separated by one base (htel$\mathbf{L}^S_3$B, htel$\mathbf{L}^S_3$H-M), was identified to efficiently catalyze the Michael addition with enantioselectivities of up to 96% *ee* (*R*) and conversions >80% (Table 2 and SI). The best-performing sequence, htel$\mathbf{L}^S_3$B

Table 2. Conversion and Enantioselectivities of Different G-Quadruplex Sequences[a]

sequence	$\mathbf{L}^S$@ loop 1	$\mathbf{L}^S$@ loop 3	salt	conversion (%)	*ee* (%)
htel$\mathbf{L}^S_2$F	2	0	KCl	75 (±2)	46 (*S*) (±1)
htel$\mathbf{L}^S_2$G	2	0	KCl	69 (±4)	29 (*R*) (±1)
htel$\mathbf{L}^S_2$H	2	0	KCl	73 (±1)	4 (*S*) (±1)
htel$\mathbf{L}^S_2$F	2	0	NaCl	78 (±7)	71 (*S*) (±2)
htel$\mathbf{L}^S_2$G	2	0	NaCl	61 (±2)	67 (*S*) (±1)
htel$\mathbf{L}^S_2$H	2	0	NaCl	67 (±2)	61 (*S*) (±1)
htel$\mathbf{L}^S_3$B	1	2	KCl	92 (±8)	96 (*R*) (±3)
htel$\mathbf{L}^S_3$D	1	2	KCl	80 (±7)	91 (*R*) (±1)
htel$\mathbf{L}^S_3$J	1	2	KCl	97 (±2)	91 (*R*) (±3)
htel$\mathbf{L}^S_3$B	1	2	NaCl	45 (±2)	55 (*R*) (±1)
htel$\mathbf{L}^S_3$D	1	2	NaCl	20 (±1)	68 (*R*) (±1)
htel$\mathbf{L}^S_3$J	1	2	NaCl	22 (±7)	52 (*R*) (±4)

[a]For further data, see the SI. Conditions: 120 μM G-quadruplex, 100 μM $CuSO_4$, 10 mM HEPES pH 8, 100 mM KCl/NaCl, 100 mM DMM, 1 mM **MA1**, and 1% v/v DMSO, 5 °C, 3 d. All experiments were performed in duplicate. The reported error is the standard deviation from two experiments.

(96% *ee* (*R*)), contained besides $\mathbf{L}^S$ only thymine in loops 1 and 3, while less active quadruplexes htel$\mathbf{L}^S_3$H-M contained one adenine in loop 1 or 3, suggesting that the formation of A-T base pairs within the loop has a negative influence on the catalytic fidelity.

Interestingly, with respect to htel$\mathbf{L}^S_3$B, changing the position of T^{18} and $\mathbf{L}^{S19}$ in loop 3 to $\mathbf{L}^{S18}$ and T^{19} led to an inversion of the enantioselectivity in htel$\mathbf{L}^S_3$C (57% *ee* (*S*)), while changing the position of $\mathbf{L}^{S17}$ and T^{18} to $\mathbf{L}^{S18}$ and T^{17} as in htel$\mathbf{L}^S_3$D had only a minor influence on the enantioselectivity (91% *ee* (*R*)). More drastic was the effect when $\mathbf{L}^S$ was incorporated twice in loop 1 and once in loop 3 (htel$\mathbf{L}^S_3$A, htel$\mathbf{L}^S_3$E, and htel$\mathbf{L}^S_3$F), leading to poor conversions (<30%) and enantioselectivities (<31% *ee*). Sequences with only two counts of $\mathbf{L}^S$ were generally showing poor *ee* values <50%, although for some sequences, including htel$\mathbf{L}^S_2$F–J, good to excellent conversions between 69 and 97% were observed (Table 2, SI Table S7).

Role of Electrolyte. To our surprise, this dramatically changed when NaCl instead of KCl was used as electrolyte. Now, sequences htel$\mathbf{L}^S_3$B, htel$\mathbf{L}^S_3$D, and htel$\mathbf{L}^S_3$H-M, each containing three $\mathbf{L}^S$, suffered a strong decrease of both conversion (≤65%) and *ee* (≤68% (*R*)). Instead, a group of three G-quadruplexes (htel$\mathbf{L}^S_2$F–H) with two $\mathbf{L}^S$ in loop 1 was now found to catalyze the formation of the opposite (*S*) enantiomer with fair *ee* (61–71%) and conversions of 61–78%. Further sequences, also containing two $\mathbf{L}^S$, but both in loop 3 or one each in loops 1 and 3, were still poorly performing. The only exception was htel$\mathbf{L}^S_2$I, with two $\mathbf{L}^S$ in loop 3, showing a modest conversion of 43% with 44% *ee* (*S*) in the presence of NaCl electrolyte. Although these values were not very high, a most interesting observation was made when KCl was used in the reaction with htel$\mathbf{L}^S_2$I, which showed a switch of enantioselectivity to the (*R*) enantiomer (71% *ee*) with a high conversion of 97%.

Circular Dichroism (CD) Studies. To shed light on the influence of the electrolyte, G-quadruplexes htel$\mathbf{L}^S_3$D and htel$\mathbf{L}^S_2$G were investigated by CD spectroscopy (Figure 2). In

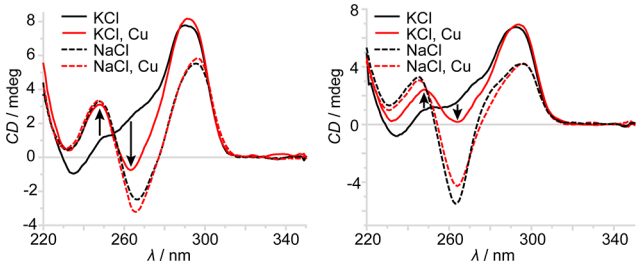

Figure 2. CD spectra of htel$\mathbf{L}^S_3$D (left) and htel$\mathbf{L}^S_2$G (right) in the absence (black) and presence (red) of Cu^{II}. Conditions: 2 μM G-quadruplex, 2 μM $CuSO_4$, 10 mM HEPES pH 8, 100 mM K/NaCl.

Na-containing solution, both sequences show the typical CD signature of an antiparallel G-quadruplex with a positive Cotton effect around ~295 nm. Addition of Cu^{II} had only minor effects on the CD signature. In contrast, with KCl used as electrolyte, the CD signature of copper-free htel$\mathbf{L}^S_3$D has a significantly different appearance, showing a striking similarity to the spectrum of a G-quadruplex in a (3 + 1) topology with two G-tetrads.[50,51] Here, addition of Cu^{II} leads to quite dramatic CD spectral changes. In accordance with our previously reported observations for a related pyridine-functionalized G-quadruplex,[43] we propose a copper-induced structural change toward a more pronounced antiparallel topology with three G-tetrads to be the reason. For htel$\mathbf{L}^S_3$D, this can be actually expected, since metal coordination to three ligands in two opposite loops should template the formation of an antiparallel topology. For htel$\mathbf{L}^S_2$G, a similar transformation of the CD spectrum is observed, albeit not in the same magnitude. Upon addition of Cu^{II}, sequence htel$\mathbf{L}^S_3$D hence shows a strong preference to fold into the same antiparallel G-quadruplex, in both NaCl and KCl solution, leading to formation of the same enantiomer (*R*) in the Michael addition. When comparing the obtained enantioselectivities for both sequences, however, it is noticeable that htel$\mathbf{L}^S_2$G forms the (*S*) enantiomer in the presence of NaCl (similar to other strands containing both ligands in loop 1) but the (*R*) product in KCl solution. We suggest two possible explanations: either htel$\mathbf{L}^S_2$G, containing both ligands in the same loop, does not fully convert into an antiparallel topology upon Cu^{II} coordination (as there is no further ligand to bridge to in another loop), or opposing enantioselectivities in the observed cases result from two distinctive antiparallel folding motifs, one of basket type, with parallel orientation of loops 1 and 3, and the other of chair type, with antiparallel loop orientation.

Overall, the results suggest that sequences with three ligands adopt rather fixed topologies, templated by the chelated Cu^{II} cations, while structures of quadruplexes with only two ligands (i.e., when situated in the same loop) are under only weak control of the rather loosely coordinated metal cation and thus more prone to changes caused by the overall sequence and electrolyte used. This hypothesis could be further supported by melting curve analysis and a series of native ESI-MS experiments, demonstrating that sequences in which Cu^{II} cations bridge ligands in opposite loops possess significantly higher gas-phase stabilities of their cation-coordinated, folded

https://dx.doi.org/10.1021/jacs.0c13251
J. Am. Chem. Soc. 2021, 143, 3555–3561

forms than those containing all ligands in the same loop (Figures S38–S42).

Comparison of Ligand Stereochemistry. Next, we examined how the stereo configuration of **L** affects the catalytic performance. Up to this point, only $\mathbf{L}^S$ was studied. Ligand $\mathbf{L}^R$ was then incorporated into the previously best-performing sequences, resulting in diastereomeric G-quadruplexes whose performances are listed in Table 3. No general

Table 3. Influence of Ligand Configuration on Conversion and Enantioselectivity[a]

sequence	L^R	electrolyte	conversion (%)	*ee* [%]
htel$\mathbf{L}^R_2$G	2	NaCl	92 (±7)	90 (*S*) (±1)
htel$\mathbf{L}^R_2$H	2	NaCl	93 (±1)	56 (*S*) (±1)
htel$\mathbf{L}^R_2$F	2	NaCl	95 (±4)	86 (*S*) (±1)
htel$\mathbf{L}^R_3$D	3	KCl	94 (±7)	≥99 (*R*) (±1)
htel$\mathbf{L}^R_3$B	3	KCl	97 (±1)	84 (*R*) (±1)
htel$\mathbf{L}^R_3$J	3	KCl	96 (±4)	85 (*R*) (±1)
htel$\mathbf{L}^R_3$H	3	KCl	95 (±1)	68 (*R*) (±1)

[a]Conditions: 120 μM G-quadruplex, 100 μM $CuSO_4$, 10 mM HEPES pH 8, 100 mM electrolyte, 100 mM DMM, 1 mM **MA1**, and 1% v/v DMSO, 5 °C, 3 d. The reported error is the standard deviation from two experiments.

influence on enantioselectivity was observed, as the same trends for the $\mathbf{L}^R$-containing sequences were observed as with $\mathbf{L}^S$. G-quadruplexes containing three ligands, one of them in loop 1 and two in loop 3, favored the formation of the (*R*) enantiomer (Figure 3d), while G-quadruplexes with two ligands in loop 1 favored the formation of the (*S*) enantiomer (Figure 3c). Two sequences (htel$\mathbf{L}^R_3$D: AGG GTL^R TGG GTT AGG GTL^{R}L^{R}GG G and htel$\mathbf{L}^R_2$G: AGG GTL^{R}L^{R}GG GTT AGG GTT AGG G) were identified with even further improved conversions and enantioselectivities (≥99% (*R*) and

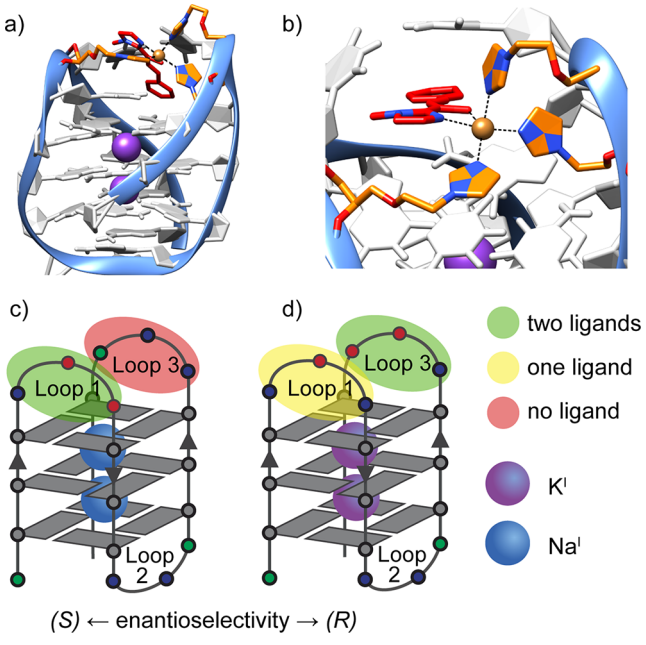

Figure 3. (a) MD simulation of htel$\mathbf{L}^R_3$D in the presence of Cu^{II} and substrate (red). (b) Zoom-in on the Cu^{II} site (for details, see the SI) and scheme of G-quadruplex properties that contribute to an enrichment of either the (c) (*S*) or (d) (*R*) enantiomer.

90 (*S*)) as compared to htel$\mathbf{L}^S_3$D and htel$\mathbf{L}^S_2$G (91% (*R*) and 67% (*S*)). The best-performing sequence htel$\mathbf{L}^R_3$D was analyzed by preliminary molecular dynamics (MD) simulations (Figure 3a,b), suggesting that neighboring nucleotides are shielding one face of the substrate for nucleophilic attack, thus giving rise to the observed enantioselectivity.

Kinetic Investigations. After identifying the most efficient sequences in terms of enantioselectivity, we investigated the kinetics of the Michael addition. For this study, sequences htel$\mathbf{L}^R_3$D, htel$\mathbf{L}^R_3$H, htel$\mathbf{L}^R_2$G, and htel$\mathbf{L}^R_2$F were chosen, as they show the best conversions. The concentration was reduced to 12 μM G-quadruplex and 10 μM Cu^{II}, corresponding to 1% active DNAzyme. To determine v_0 and k_{cat}, the onset of product formation was plotted against the time and fitted via linear regression, and v_0 was determined. Dividing v_0 by the concentration of the active DNAzyme gave k_{cat}.

While for Cu^{II} alone a reaction rate v_0 = 2 μM h^{-1} was determined, the rate significantly increased in the presence of htel$\mathbf{L}^R_3$H and htel$\mathbf{L}^R_2$G to v_0 = 4 and 9 μM h^{-1}, respectively (Figure 4). For htel$\mathbf{L}^R_3$D, an even further increase was

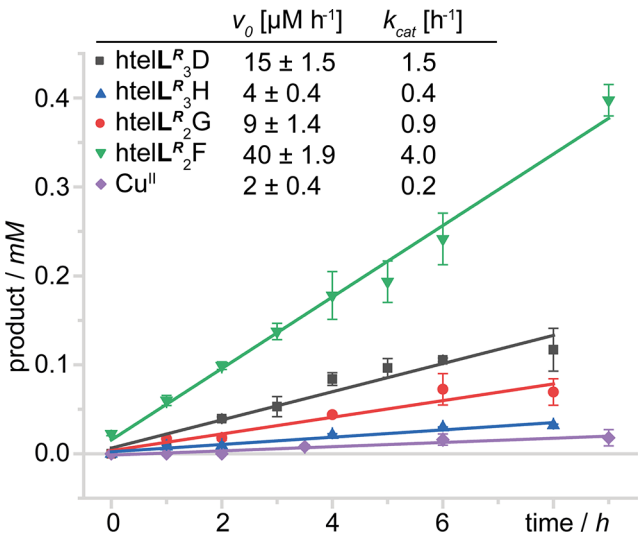

Figure 4. Time-dependent onset of product formation for Cu(II) complexes of htel$\mathbf{L}^R_3$D, htel$\mathbf{L}^R_3$H, htel$\mathbf{L}^R_2$G, htel$\mathbf{L}^R_2$F and free Cu^{II}. Every data point is the average of two independent experiments. Conditions: 12 μM G-quadruplex, 10 μM $CuSO_4$, 10 mM HEPES pH 8, 100 mM KCl (three $\mathbf{L}^R$) or NaCl (two $\mathbf{L}^R$), 100 mM DMM, 1 mM **MA1**, and 1% v/v DMSO, 5 °C.

observed (v_0 = 15 μM h^{-1}), but most remarkably, htel$\mathbf{L}^R_2$F showed a reaction rate of v_0 = 40 μM h^{-1}, a 20-fold increase compared to that obtained with Cu^{II} alone.

To explain these findings, we took a deeper look at the loop compositions. For htel$\mathbf{L}^R_3$D (v_0 = 15 μM h^{-1}) and htel$\mathbf{L}^R_3$H (v_0 = 4 μM h^{-1}), only the latter quadruplex contains an adenine in loop 1, likely to interact with a thymine in loop 2 to form a loose A-T base pair. Such a hydrogen-bonded interaction across the cavity created by the loops may hinder substrate access to the catalytic metal site and hence be responsible for the diminished reaction rate. This explanation might also be valid for sequences htel$\mathbf{L}^R_2$F (v_0 = 40 μM h^{-1}) and htel$\mathbf{L}^R_2$G (v_0 = 9 μM h^{-1}) where, most interestingly, the only difference is an inverted sequence of loop 1 in htel$\mathbf{L}^R_2$F ($\mathbf{L}^R\mathbf{L}^R$T) as compared to htel$\mathbf{L}^R_2$G (TL^{R}L^R). We speculate that only htel$\mathbf{L}^R_2$G can form an A-T base pair with an adenine in

https://dx.doi.org/10.1021/jacs.0c13251
J. Am. Chem. Soc. 2021, 143, 3555−3561

the oppositely arranged loop 3, again leading to deceleration of the catalytic reaction. Notably, the assumptions made herein based on kinetic data are in good agreement with the above-mentioned trends for conversion and enantioselectivity dependent on the contained adenines and thymines. Such indications for base-pairing within the loops should count as important considerations for the optimization of sequences in future studies.

Next, we wondered whether our system shows Michaelis–Menten-type kinetics, a prominent feature of natural enzymes. To accurately analyze this, we made sure that substrate **MA1** was completely dissolved, allowing us to investigate a series of Cu^{II}-htel$\mathbf{L}^{R}_{3}$D-catalyzed Michael addition experiments with increasing substrate concentrations (2.5–45 μM). For this purpose, 10% DMSO was added, and the temperature was increased to 25 °C (hence, the obtained reaction rates cannot be directly compared to the values described above). The reaction was followed by the change of absorption at 336 nm, considering that only **MA1** is contributing to the absorption at this wavelength. From the slope, reaction rate v was calculated, plotted against the substrate starting concentration, and fitted using a typical Michaelis–Menten kinetics model (see SI for details). A value of K_M = 35.2 μM (v_{max} = 8.2 nM min^{-1}) was determined for the reaction catalyzed by Cu^{II}-htel$\mathbf{L}^{R}_{3}$D (SI, Figure S28a, black curve), while no Michaelis–Menten behavior could be observed for the reaction catalyzed by free Cu^{II} cations.

Screen of Substrate Scope. To show the generality of the approach, the two sequences featuring the highest observed enantioselectivities, htel$\mathbf{L}^{R}_{2}$G and htel$\mathbf{L}^{R}_{3}$D, were investigated for transforming a wider scope of substrates, involving electron-rich and -poor as well as bulky Michael acceptors (Table 4). Substrate **MA2**, with a nitro group in the *para* position, was shown to poorly react, and conversions of only 17% (htel$\mathbf{L}^{R}_{2}$G) and 34% (htel$\mathbf{L}^{R}_{3}$D) were observed. Both the very low solubility of substrate **MA2** and electron-withdrawing character of the $-NO_2$ group could be responsible for this result. A deactivating effect was also observed for substrate **MA5**, carrying another electron-withdrawing substituent ($-CF_3$), for which low conversions of 73% (htel$\mathbf{L}^{R}_{2}$G) and 59% (htel$\mathbf{L}^{R}_{3}$D) were obtained, but with good enantioselectivities of 90% (+) (htel$\mathbf{L}^{R}_{2}$G) and 98% (−) (htel$\mathbf{L}^{R}_{3}$D). In agreement with these results, electron-rich substrates **MA3** (4-OCH_3) and **MA6** (4-CH_3) yielded higher conversions, especially for substrate **MA6**, with conversions of >94% for both sequences and excellent enantioselectivities of up to 99% (−). A bulky *tert*-butyl group in **MA4** resulted in a lower reactivity, but interestingly, with htel$\mathbf{L}^{R}_{2}$G, the best enantioselectivity of 95% (+) was observed among all substrates. For **MA7**, where *N*-methyl-imidazole was replaced with pyridine, excellent conversions of >97% for both sequences were obtained, but also a decrease of their enantioselectivities to 71% (+) (htel$\mathbf{L}^{R}_{2}$G) and 90% (−) (htel$\mathbf{L}^{R}_{3}$D). Interestingly, for all investigated substrates, again htel$\mathbf{L}^{R}_{2}$G enriched the first-eluting (+) enantiomer, while htel$\mathbf{L}^{R}_{3}$D enriched the (−) enantiomer. Although the absolute stereoconfiguration was not individually determined for products resulting from **MA2–7**, this suggests that the G-quadruplex properties governing the formation of (*R*) or (*S*) enantiomers with **MA1** are the same for all other investigated substrates.

Table 4. Conversion and Enantioselectivities for Michael Acceptors MA1–7[a]

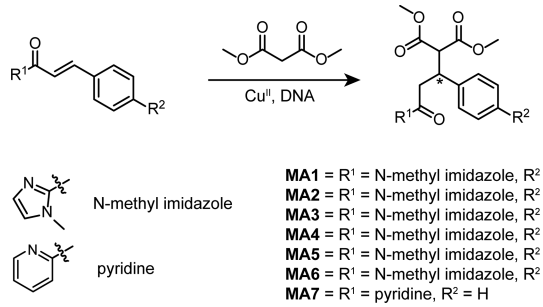

sequence	electrolyte	substrate	conversion (%)	*ee* (%)
htel$\mathbf{L}^{R}_{2}$G	NaCl	**MA1**	92 (±7)	90 (*S*) (±1)
htel$\mathbf{L}^{R}_{2}$G	NaCl	**MA2**	17 (±1)	77 (+) (±1)
htel$\mathbf{L}^{R}_{2}$G	NaCl	**MA3**	94 (±3)	81 (+) (±1)
htel$\mathbf{L}^{R}_{2}$G	NaCl	**MA4**[#]	67 (±4)	95 (+) (±1)
htel$\mathbf{L}^{R}_{2}$G	NaCl	**MA5**	73 (±5)	90 (+) (±2)
htel$\mathbf{L}^{R}_{2}$G	NaCl	**MA6**	94 (±2)	89 (+) (±2)
htel$\mathbf{L}^{R}_{2}$G	NaCl	**MA7**	98 (±1)	71 (+) (±3)
htel$\mathbf{L}^{R}_{3}$D	KCl	**MA1**	94 (±7)	≥99 (*R*) (±1)
htel$\mathbf{L}^{R}_{3}$D	KCl	**MA2**	34 (±2)	75 (−) (±3)
htel$\mathbf{L}^{R}_{3}$D	KCl	**MA3**	90 (±8)	98 (−) (±1)
htel$\mathbf{L}^{R}_{3}$D	KCl	**MA4**[#]	74 (±8)	86 (−) (±6)
htel$\mathbf{L}^{R}_{3}$D	KCl	**MA5**	59 (±9)	98 (−) (±1)
htel$\mathbf{L}^{R}_{3}$D	KCl	**MA6**	99 (±1)	99 (−) (±1)
htel$\mathbf{L}^{R}_{3}$D	KCl	**MA7**	97 (±3)	90 (−) (±1)

[a]Conditions: 120 μM DNA, 100 μM $CuSO_4$, 10 mM HEPES pH 8, 100 mM electrolyte, 100 mM DMM, 1 mM substrate, and 1% v/v DMSO, 5 °C, 3 d. All experiments were performed in duplicate. The reported error is the standard deviation from two experiments. [#]4% v/v DMSO.

CONCLUSIONS

A new modular approach for the rational design of Cu^{II}-dependent metalloDNAzymes was introduced. The modification of $htel_{22}$ with imidazole-based ligandoside **L** led to the design of highly efficient Cu^{II}-based catalysts for the enantioselective Michael addition. Iterative rounds of screening and sequence design unveiled crucial structure–function relationships, enabling the optimization of DNAzymes for obtaining both enantiomeric products. For the (*S*) enantiomer, two ligands have to be incorporated in loop 1, while for the (*R*) enantiomer, one ligand is placed in loop 1 and two in loop 3. Besides, the electrolyte composition was also found to control enantioselectivity.

Interestingly, the stereoconfiguration of the ligand itself ($\mathbf{L}^{S}$ and $\mathbf{L}^{R}$) had only a minor impact, although htel$\mathbf{L}^{R}_{2}$G (92% conv., 90% *ee* (*S*)) and htel$\mathbf{L}^{R}_{3}$D (94% conv., ≥99% *ee* (*R*)) were identified as the best-performing sequences. The general applicability of the approach was shown for a larger substrate scope, including ones with electron-poor and -rich as well as bulky substituents and a pyridine. For most of the investigated substrates, good to excellent conversions with high enantioselectivities were observed, although electron-withdrawing substituents led to lower reactivities. Kinetic studies identified htel$\mathbf{L}^{R}_{2}$F as the most efficient DNAzyme in the presence of Cu^{II} cations, accelerating the reaction 20-fold compared to that with free Cu^{II}. For htel$\mathbf{L}^{R}_{3}$D, Michaelis–Menten kinetics were elucidated, showing v_{max} = 8.2 nM min^{-1} with a corresponding

https://dx.doi.org/10.1021/jacs.0c13251
J. Am. Chem. Soc. 2021, 143, 3555–3561

K_M = 35.2 μM. The herein introduced system serves as a versatile platform for the development of novel metallo-DNAzymes, enabling the systematic optimization of catalysts for a variety of reactions. Required oligonucleotides contain a synthetically simple modification and are readily accessible via automated DNA synthesis.

■ ASSOCIATED CONTENT

Supporting Information

The Supporting Information is available free of charge at https://pubs.acs.org/doi/10.1021/jacs.0c13251.

Synthetic procedures, NMR, MS, UV−vis, CD, and HPLC data, and MD simulations, including Figures S1−S47 and Tables S1−S15 (PDF)

■ AUTHOR INFORMATION

Corresponding Author

Guido H. Clever − *Faculty of Chemistry and Chemical Biology, TU Dortmund University, 44227 Dortmund, Germany*; orcid.org/0000-0001-8458-3060; Email: guido.clever@tu-dortmund.de

Authors

Philip M. Punt − *Faculty of Chemistry and Chemical Biology, TU Dortmund University, 44227 Dortmund, Germany*

Marie D. Langenberg − *Faculty of Chemistry and Chemical Biology, TU Dortmund University, 44227 Dortmund, Germany*

Okan Altan − *Faculty of Chemistry and Chemical Biology, TU Dortmund University, 44227 Dortmund, Germany*

Complete contact information is available at: https://pubs.acs.org/10.1021/jacs.0c13251

Notes

The authors declare no competing financial interest.

■ ACKNOWLEDGMENTS

Funded by the Deutsche Forschungsgemeinschaft (DFG, German Research Foundation) under Germany's Excellence Strategy, EXC 2033-390677874-RESOLV.

■ REFERENCES

(1) Holm, R. H.; Kennepohl, P.; Solomon, E. I. Structural and Functional Aspects of Metal Sites in Biology. *Chem. Rev.* **1996**, *96*, 2239.

(2) Brandenberg, O. F.; Fasan, R.; Arnold, F. H. Exploiting and Engineering Hemoproteins for Abiological Carbene and Nitrene Transfer Reactions. *Curr. Opin. Biotechnol.* **2017**, *47*, 102.

(3) Drienovská, I.; Rioz-Martínez, A.; Draksharapu, A.; Roelfes, G. Novel Artificial Metalloenzymes by in Vivo Incorporation of Metal-Binding Unnatural Amino Acids. *Chem. Sci.* **2015**, *6*, 770.

(4) Key, H. M.; Dydio, P.; Clark, D. S.; Hartwig, J. F. Abiological Catalysis by Artificial Haem Proteins Containing Noble Metals in Place of Iron. *Nature* **2016**, *534*, 534.

(5) Zhao, J.; Bachmann, D. G.; Lenz, M.; Gillingham, D. G.; Ward, T. R. An Artificial Metalloenzyme for Carbene Transfer Based on a Biotinylated Dirhodium Anchored within Streptavidin. *Catal. Sci. Technol.* **2018**, *8*, 2294.

(6) Srivastava, P.; Yang, H.; Ellis-Guardiola, K.; Lewis, J. C. Engineering a Dirhodium Artificial Metalloenzyme for Selective Olefin Cyclopropanation. *Nat. Commun.* **2015**, *6*, 7789.

(7) Drienovská, I.; Mayer, C.; Dulson, C.; Roelfes, G. A Designer Enzyme for Hydrazone and Oxime Formation Featuring an Unnatural Catalytic Aniline Residue. *Nat. Chem.* **2018**, *10*, 946.

(8) Hestericová, M.; Heinisch, T.; Alonso-Cotchico, L.; Maréchal, J.; Vidossich, P.; Ward, T. R. Directed Evolution of an Artificial Imine Reductase. *Angew. Chem., Int. Ed.* **2018**, *57*, 1863.

(9) Jeschek, M.; Reuter, R.; Heinisch, T.; Trindler, C.; Klehr, J.; Panke, S.; Ward, T. R. Directed Evolution of Artificial Metalloenzymes for in Vivo Metathesis. *Nature* **2016**, *537*, 661.

(10) Breaker, R. R.; Joyce, G. F. A DNA Enzyme That Cleaves RNA. *Chem. Biol.* **1994**, *1*, 223.

(11) Cuenoud, B.; Szostak, J. W. A DNA Metalloenzyme with DNA Ligase Activity. *Nature* **1995**, *375*, 611.

(12) Cheng, M.; Li, Y.; Zhou, J.; Jia, G.; Lu, S.-M.; Yang, Y.; Li, C. Enantioselective Sulfoxidation Reaction Catalyzed by a G-quadruplex DNA Metalloenzyme. *Chem. Commun.* **2016**, *52*, 9644.

(13) Li, Y.; Sen, D. A Catalytic DNA for Porphyrin Metallation. *Nat. Struct. Mol. Biol.* **1996**, *3*, 743.

(14) Sengle, G.; Eisenführ, A.; Arora, P. S.; Nowick, J. S.; Famulok, M. Novel RNA Catalysts for the Michael Reaction. *Chem. Biol.* **2001**, *8*, 459.

(15) Le Vay, K.; Salibi, E.; Song, E. Y.; Mutschler, H. Nucleic Acid Catalysis under Potential Prebiotic Conditions. *Chem. - Asian J.* **2020**, *15*, 214.

(16) Xu, Y.; Suzuki, Y.; Lönnberg, T.; Komiyama, M. Human Telomeric DNA Sequence-Specific Cleaving by G-Quadruplex Formation. *J. Am. Chem. Soc.* **2009**, *131*, 2871.

(17) Golub, E.; Albada, H. B.; Liao, W.-C.; Biniuri, Y.; Willner, I. Nucleoapzymes: Hemin/G-Quadruplex DNAzyme−Aptamer Binding Site Conjugates with Superior Enzyme-like Catalytic Functions. *J. Am. Chem. Soc.* **2016**, *138*, 164.

(18) Huang, P. J.; Rochambeau, D.; Sleiman, H. F.; Liu, J. Target Self-Enhanced Selectivity in Metal-Specific DNAzymes. *Angew. Chem.* **2020**, *132*, 3601.

(19) Marek, J. J.; Singh, R. P.; Heuer, A.; Hennecke, U. Enantioselective Catalysis by Using Short, Structurally Defined DNA Hairpins as Scaffold for Hybrid Catalysts. *Chem. - Eur. J.* **2017**, *23*, 6004.

(20) Boersma, A. J.; Feringa, B. L.; Roelfes, G. Enantioselective Friedel−Crafts Reactions in Water Using a DNA-Based Catalyst. *Angew. Chem., Int. Ed.* **2009**, *48*, 3346.

(21) Roelfes, G.; Feringa, B. L. DNA-Based Asymmetric Catalysis. *Angew. Chem., Int. Ed.* **2005**, *44*, 3230.

(22) Park, S.; Matsui, H.; Fukumoto, K.; Yum, J. H.; Sugiyama, H. Histidine-Conjugated DNA as a Biomolecular Depot for Metal Ions. *RSC Adv.* **2020**, *10*, 9717.

(23) Mansot, J.; Lauberteaux, J.; Lebrun, A.; Mauduit, M.; Vasseur, J.-J.; Marcia de Figueiredo, R.; Arseniyadis, S.; Campagne, J.-M.; Smietana, M. DNA-Based Asymmetric Inverse Electron-Demand Hetero-Diels−Alder. *Chem. - Eur. J.* **2020**, *26*, 3519.

(24) Roe, S.; Ritson, D. J.; Garner, T.; Searle, M.; Moses, J. E. Tuneable DNA-based Asymmetric Catalysis using a G-quadruplex Supramolecular Assembly. *Chem. Commun.* **2010**, *46*, 4309.

(25) Wang, C.; Jia, G.; Zhou, J.; Li, Y.; Liu, Y.; Lu, S.; Li, C. Enantioselective Diels−Alder Reactions with G-Quadruplex DNA-Based Catalysts. *Angew. Chem., Int. Ed.* **2012**, *51*, 9352.

(26) Hao, J.; Miao, W.; Cheng, Y.; Lu, S.; Jia, G.; Li, C. Enantioselective Olefin Cyclopropanation with G-Quadruplex DNA-Based Biocatalysts. *ACS Catal.* **2020**, *10*, 6561.

(27) Wang, C.; Li, Y.; Jia, G.; Liu, Y.; Lu, S.; Li, C. Enantioselective Friedel−Crafts Reactions in Water Catalyzed by a Human Telomeric G-quadruplex DNA Metalloenzyme. *Chem. Commun.* **2012**, *48*, 6232.

(28) Wang, C.; Jia, G.; Li, Y.; Zhang, S.; Li, C. Na + /K + Switch of Enantioselectivity in G-quadruplex DNA-based Catalysis. *Chem. Commun.* **2013**, *49*, 11161.

(29) Yum, J. H.; Park, S.; Sugiyama, H. G-quadruplexes as Versatile Scaffolds for Catalysis. *Org. Biomol. Chem.* **2019**, *17*, 9547.

(30) Dey, S.; Jäschke, A. Tuning the Stereoselectivity of a DNA-Catalyzed Michael Addition through Covalent Modification. *Angew. Chem., Int. Ed.* **2015**, *54*, 11279.

(31) Jash, B.; Müller, J. A Stable Zinc(II)-Mediated Base Pair in a Parallel-Stranded DNA Duplex. *J. Inorg. Biochem.* **2018**, *186*, 301.

(32) Katz, S. The Reversible Reaction of Hg (II) and Double-Stranded Polynucleotides a Step-Function Theory and Its Significance. *Biochim. Biophys. Acta, Spec. Sect. Nucleic Acids Relat. Subj.* **1963**, *68*, 240.
(33) Clever, G. H.; Polborn, K.; Carell, T. A Highly DNA-Duplex-Stabilizing Metal−Salen Base Pair. *Angew. Chem., Int. Ed.* **2005**, *44*, 7204.
(34) Johannsen, S.; Megger, N.; Böhme, D.; Sigel, R. K. O.; Müller, J. Solution Structure of a DNA Double Helix with Consecutive Metal-Mediated Base Pairs. *Nat. Chem.* **2010**, *2*, 229.
(35) Tanaka, K.; Clever, G. H.; Takezawa, Y.; Yamada, Y.; Kaul, C.; Shionoya, M.; Carell, T. Programmable Self-Assembly of Metal Ions inside Artificial DNA Duplexes. *Nat. Nanotechnol.* **2006**, *1*, 190.
(36) Duprey, J. H. A.; Takezawa, Y.; Shionoya, M. Metal-Locked DNA Three-Way Junction. *Angew. Chem., Int. Ed.* **2013**, *52*, 1212.
(37) Takezawa, Y.; Maeda, W.; Tanaka, K.; Shionoya, M. Discrete Self-Assembly of Iron(III) Ions inside Triple-Stranded Artificial DNA. *Angew. Chem., Int. Ed.* **2009**, *48*, 1081.
(38) Abdelhamid, M. A.; Fábián, L.; MacDonald, C. J.; Cheesman, M. R.; Gates, A. J.; Waller, Z. A. Redox-Dependent Control of i-Motif DNA Structure Using Copper Cations. *Nucleic Acids Res.* **2018**, *46*, 5886.
(39) Engelhard, D. M.; Pievo, R.; Clever, G. H. Reversible Stabilization of Transition-Metal-Binding DNA G-Quadruplexes. *Angew. Chem., Int. Ed.* **2013**, *52*, 12843.
(40) Miyoshi, D.; Karimata, H.; Wang, Z.-M.; Koumoto, K.; Sugimoto, N. Artificial G-Wire Switch with 2,2'-Bipyridine Units Responsive to Divalent Metal Ions. *J. Am. Chem. Soc.* **2007**, *129*, 5919.
(41) Neidle, S. Quadruplex Nucleic Acids as Targets for Anticancer Therapeutics. *Nat. Rev. Chem.* **2017**, *1*, 0041.
(42) Spiegel, J.; Adhikari, S.; Balasubramanian, S. The Structure and Function of DNA G-Quadruplexes. *Trends Chem.* **2020**, *2*, 123.
(43) Engelhard, D. M.; Nowack, J.; Clever, G. H. Copper-Induced Topology Switching and Thrombin Inhibition with Telomeric DNA G-Quadruplexes. *Angew. Chem., Int. Ed.* **2017**, *56*, 11640.
(44) Engelhard, D. M.; Stratmann, L. M.; Clever, G. H. Structure−Property Relationships in CuII-Binding Tetramolecular G-Quadruplex DNA. *Chem. - Eur. J.* **2018**, *24*, 2117.
(45) Engelhard, D. M.; Meyer, A.; Berndhäuser, A.; Schiemann, O.; Clever, G. H. Di-Copper(II) DNA G-Quadruplexes as EPR Distance Rulers. *Chem. Commun.* **2018**, *54*, 7455.
(46) Punt, P. M.; Clever, G. H. Imidazole-Modified G-Quadruplex DNA as Metal-Triggered Peroxidase. *Chem. Sci.* **2019**, *10*, 2513.
(47) Punt, P. M.; Clever, G. H. Tailored Transition-Metal Coordination Environments in Imidazole-Modified DNA G-Quadruplexes. *Chem. - Eur. J.* **2019**, *25*, 13987.
(48) Punt, P. M.; Stratmann, L. M.; Sevim, S.; Knauer, L.; Strohmann, C.; Clever, G. H. Heteroleptic Coordination Environments in Metal-Mediated DNA G-Quadruplexes. *Front. Chem.* **2020**, *8*, 26.
(49) Coquière, D.; Feringa, B. L.; Roelfes, G. DNA-Based Catalytic Enantioselective Michael Reactions in Water. *Angew. Chem., Int. Ed.* **2007**, *46*, 9308.
(50) Lim, K. W.; Amrane, S.; Bouaziz, S.; Xu, W.; Mu, Y.; Patel, D. J.; Luu, K. N.; Phan, A. T. Structure of the Human Telomere in K + Solution: A Stable Basket-Type G-Quadruplex with Only Two G-Tetrad Layers. *J. Am. Chem. Soc.* **2009**, *131*, 4301.
(51) Luu, K. N.; Phan, A. T.; Kuryavyi, V.; Lacroix, L.; Patel, D. J. Structure of the Human Telomere in K+ Solution: An Intramolecular (3 + 1) G-Quadruplex Scaffold. *J. Am. Chem. Soc.* **2006**, *128*, 9963.

https://dx.doi.org/10.1021/jacs.0c13251
J. Am. Chem. Soc. 2021, 143, 3555−3561